Available online at www.sciencedirect.com

ScienceDirect

Ciência & Tecnologia dos Materiais 29 (2017) 14–21

http://ees.elsevier.com/ctmat

On the influence of porosity and pore size on AlSi17 alloy foam using artificial neural network

Dipen Kumar Rajak[a,b,*], L.A. Kumaraswamidhas[a,b], S. Das[c]

[a]*Department of Mining Machinery Engineering, Indian Institute of Technology (ISM), Dhanbad 826004, JH (India)*
[b]*Advanced Research Lab, Indian Institute of Technology (ISM), Dhanbad 826004, JH (India)*
[c]*CSIR-Advanced Materials and Processes Research Institute, Bhopal 462064, MP (India)*

Abstract

In the present investigation, AlSi17 Aluminum alloy closed-cell foam is fabricated through Melt route process using Calcium powder as thickening agent and Titanium hydride as foaming agent along with the addition of 10wt% Silicon Carbide particles. The effect of pore and pore size on the deformation mechanism under static loading conditions is studied. Also, the fabricated foam properties are analyzed after the completion of the test. The strain rate loading conditions of the compression test conducted on the Al foam lies in the range of $10^{-3}s^{-1}$ to $10s^{-1}$ and the above investigations are carried out according to the loading conditions. The Artificial Neural Artwork (ANN) approach is employed for predicting the compressive deformation of the fabricated Al alloy foam using simulations. The Plateau stress data is obtained from the compression tests and the neural network functions are successively modeled and later the specific energy absorption (SEA) is calculated from the plateau stress. The simulation results of the ANN are in good agreement with the compression test results and the predictions are performed with highest accuracy.

Keywords: plateau stress; energy absorption; porosity; relative density; artificial neural network.

1. Introduction

The defined characteristic of the commonly available aluminum foam is its usefulness as a light weight material. Due to its light weight, high strength and good stiffness, it is more suitable for crash energy absorption. Several times, it has been observed that the aluminum foam is filled with metal tube in its outer core, i.e. foam filled structure is used in different energy absorption applications [1-3]. Basically aluminum foam is classified into two categories (i) Open Cell, (ii) Closed Cell. Closed cell foams do not have interconnected pores. Normally the closed cell foams have higher compressive strength due to their structures. However, closed cell foams are also generally denser, require more material, and consequentially more expensive to produce. The closed cells can be filled with a specialized gas to provide improved insulation. The closed cell structure foams have higher dimensional stability, low moisture absorption coefficients and higher strength compared to open cell structured foams. Open-cell metal foams are composed of interconnected pores. Since a fluid can circulate through the material, they are best fitted for heat transfer. Open cell structured foams contain pores that are connected to each other and form an interconnected network which is relatively soft. Open cell foams will fill with whatever they are surrounded with. If filled with air this could be a relatively good insulator, but if the open cells are filled with water, insulation properties would be reduced. Foam rubber is a type of open cell foam. All types of foam are widely used as core material in sandwich structured composite material [7]. Now days the closed cell aluminum foam is generally used for compression load action as it has some good mechanical properties i.e. low density range, average diameter of cell [1-5].

* Corresponding author.
E-mail address: dipen.pukar@gmail.com (Dipen Kumar Rajak)

http://dx.doi.org/10.1016/j.ctmat.2017.05.004

Basically there are nine methods to produce the aluminum foam, but gradually new techniques and improved methodologies are introduced for better and cheaper production. Initially melt-route processes were employed to produce the closed cell aluminum foam commercially. Mechanical behavior of composite matrix material was modelled using artificial network [6]. Mechanical properties were predicted to ceramic tool based on artificial neural network by Huang et al [8]. Artificial neural networks (ANN) are broadly known as a technology to tackle complex and ill-definitive problems. They are particularly useful in modeling non-linear problems, where analytical solutions gets rather complex and time taking. In such case, neural network is called as non-linear statistical data modeling tool. Also the compressive properties, such as, plateau stress, Young's modulus and energy absorption characteristics of closed cell Al foams studied by using structural properties of foams are given as input to the ANN system. The results of the ANN were found to be in good agreement with the experiment data. It was also found that these ANN models help the foam manufacturers to prepare a particular database of the foam properties [5]. They learn from the examples by constructing an input-output mapping. An artificial neural network (ANN) is an alternative way to challenge complex and ill-definitive problems. Neural network is the same as non-linear statistical data modeling tool having capability to learn and simplify by simulating realistic outputs for inputs. They work with the help of input–output mapping [5-6,8,9-16]. An ANN model was developed to study the association between metallic alloy composition, its micro-structure and its stretchable properties. The developed model may be used for predicting compression properties and to optimize the processing parameters [17-28].

In this work, melt route technique is used for making aluminum alloy foam and the melt viscosity is controlled by the addition of Ca thickening and TiH_2 as foaming agent. This paper focused on the study of compression properties of AAFs with relative densities ranging from 0.26 to 0.37 and with an average pore diameter, its variation ranging from 1.1 mm to 1.8 mm using ANN model prediction. The input variables are strain rate, average pore diameter and relative density. AAN models are developed only for predicting the plateau stress (σ_{pl}), capacity depending on the input variables. The aim of this illustrated work is to study the developed AAN model under which experimental analysis was carried out to describe the energy absorption behaviour of aluminum alloy foam in quasi-statics axial deformation.

2. Experimental methodology

2.1. Microstructural analysis

Small piece of 10 mm x 10 mm were cut from the foam billets for microstructural observation of foam sample. The cut pieces were cold mounted in such a way that the exposed cells were filled with the cold mounting materials in order to avoid damaging of cell walls during grinding and polishing. The polished samples were etched with Keller's reagent. The microstructures were examined under field emission scanning electron microscope (FE-SEM; Model: Supra 55, Carl Zeiss, Germany). Etched samples were sputtered with a thin layer of platinum prior to FE-SEM observations. The micro-architectural characteristics of foam were studied by quantitative metallographic and image analysis technique. Figure 1 show the pore size distribution of AlSi17 alloy foam having 78% pores in the 0.5-1.5 mm range. This was captured using Material Pro Software [7, 12].

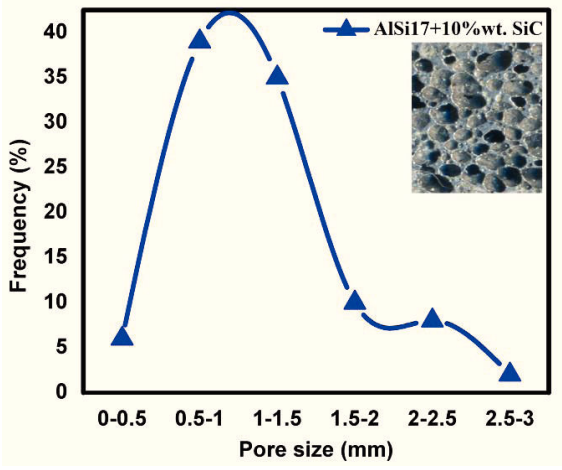

Fig. 1. Pore size distribution as a function of the number of cell pores for AlSi17 AAFs with 10% SiC.

2.2. Compression test

Square samples of size 20 mm x 20 mm x 25 mm were used for compression testing of AlSi17 alloy foam. The foam samples were finally cut with slow speed diamond cutter to avoid cell loss and wall thickening. All sample tests were carried out using a universal testing machine (INSTRON: 8801) at strain

rate of $10^{-3}s^{-1}$ to $10s^{-1}$. In the meantime, the load-displacement data was recorded and it was converted to stress-strain graph. Plateau stress (σps), and energy absorption (Ev) of these materials determined from compression stress-strain curves [4,7] were compared with each other.

3. Results and discussion

3.1. Porosity and pore geometries

Porosity was the vital parameter of the foam materials, to expose during volume fraction of the pores as an eventual product. The foam porosity was calculated from the mass (m) and volume (v) of the sample. Other significant parameters were pore size of this material. Porosity and pore size were difficult to assign for microstructure using the traditional approach due to pore size distribution of foam, it was also analyzed the size of the individual pore of the foam sample found on the outer side was purposive by software perusal. The small slice of foam sample was being taken to determine the pore size. It is noted that the cell wall thickness of AAFs is varied from the length of casting billet and foaming temperature. The density of foam depends upon the some basic processes parameters i.e. thickening agent and foaming hydride power, which in turn has influenced the porosity and pore size. Figure 2 (a) shows the top portion of foam slice, (b) indicates the middle portion, and (c) shows the bottom portion of billet slice. Figure 3(a) and (b) gives the pore structure, hence the pore structure depends on balancing the viscosity and interfacial energy of foaming liquid and presence of pressure difference between cell throughout the processing of foam. Basically the aluminum alloy liquid system exhibits the high interfacial energy, after making foam, the cell wall instantly breaks because of presence of high surface tension in liquid.

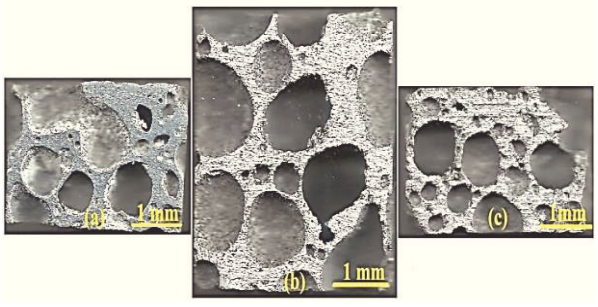

Fig. 2. Thickness of the dense surface in different portion of AlSi17 Al-alloy foam: (a) Top surface, (b) Middle surface, (c) Bottom surface.

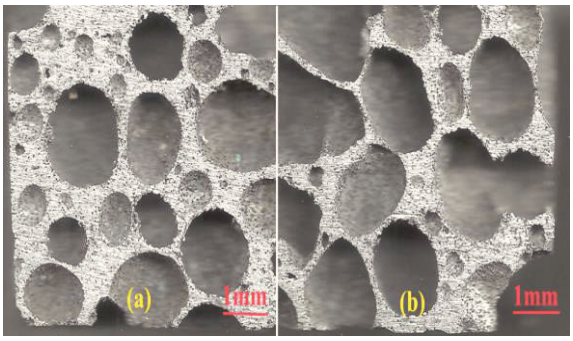

Fig. 3. Pore geometries: (a) spherical, (b) polyhedral shape of AlSi17 Al-alloy foam.

If the pressure is increased in the foaming processes then also the cell size will decrease [26-28].

3.2. Microstructure characterization and energy dispersive X-ray analysis (EDXA)

Microstructure of SiC used in making AAFs shows that the SiC particles are perfectly aligned with the average cell wall thickness of this foam. The TiH_2 powder with average particle size range of 20–55μm and 44 μm mean size has been used as foaming agent. The micro structural analysis has been carried out in this investigation to explore about the characteristics of the Al alloy composite foams for the forty five work piece. The optimal electronic microscope is used to examine the micro structure; the Keller's etchant (Distilled water Nitric acid Hydrochloric acid Hydrofluoric acid) is applied on the upper surface in correct proportion to expose their grain structure and orientations of work piece of foam slice, is displayed in Figure 1 [4,6,19]. The micro structural analysis carried is out to obtain the optical micrographs in low and high magnification of the Al alloy composite foam to understand the wall thickness and distribution characterization of SiC particles. In this study, various micrographs have been discussed in Figure 4 and 5. Magnified view of micrograph of the cell wall of AAFs is shown in Figure 4(a) and Figure 4 (b) shows the microstructure of AlSi17+10%wt SiCp composite with uniform distribution of SiC particles and reasonably good bonding between SiC and the matrix. It can clearly observed that Figure 4 identifies the two different zones. It is evident that the cell wall of AAFs contains SiC particles, uniformly distributed in the matrix (under circle marked) over the cell wall of Al alloy composite foam.

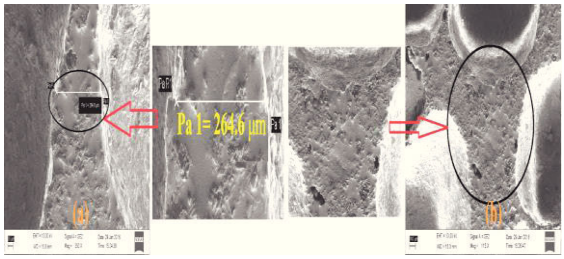

Fig. 4. (a) and (b) reveal the microstructure behavior of AAFs by FE-SEM technique.

These cell walls are dense in nature. This is because of the fact the bubble size normally depends on melt viscosity and surface tension which are primarily governed by the melt temperature and the amount of thickening agent used. However, cell wall's thickness decreases with increase in TiH_2 concentration used for foaming. As the number of cells increases and the cell size remained unchanged, it is expected that volume fraction of porosity will increase with increase in TiH_2 concentration and the cell wall's thickness will decrease. Figure 5 shows the energy dispersive X-ray analysis (EDXA) at various locations. This figure indicates the existence of intermetallic and oxides on the cell wall of aluminum alloy (AlSi17) foam [19].

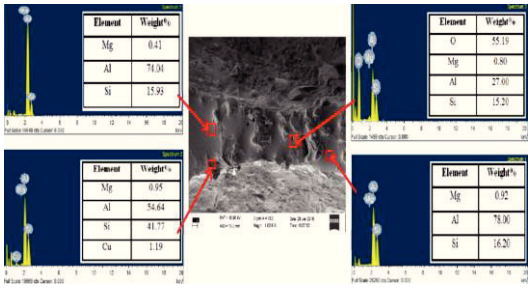

Fig. 5. Microstructure of AlSi17 alloy foam cell wall with EDAX analysis at different point.

3.3. Compression deformation and energy absorption mechanism

The compression deformation behavior was studied by analyzing the compressive stress-strain diagram of AAFs. Experimentally it is witnessed for each sample that foam sample follows regular deformation mechanism, no sample is seen to go out of general deformation pattern. During the whole sample testing no sample faced unpredictable buckling failure. So it is noted that AAFs are not affected by deformation mechanism. The present work has investigated the plateau stress of aluminum alloy foam (AlSi17 with 10wt% SiCp) and the potential of a neural network approach to correlate and predict its performance with the testing condition. Effect of various input parameters, i.e., average pore size, strain rate and relative density have been considered for the present study purpose. The range of these parameters is predicted in Table 1. In this step, three same samples were prepared for each state and later tests or investigations are applied to all the samples to avoid accidental errors".

Table 1. Parameters used for ANN formulation.

Sl. No	Significant Parameter	Parameters Range
1	Average pore Diameters (mm)	1.1-1.9
2	strain rate (s^{-1})	0.001-10
3	Relative density	0.29-0.34

The compression stress-strain curve of AAFs at a strain rate of $10^{-2}s^{-1}$ with relative density (RD = 0.29) and all the three regions as generally observed in conventional foam material are shown in Figure 6(a).The plateau stress (σ_{pl}) is considered to be the average stress in plateau region and its increase with increase in RD. It is evident that the dense composite does not show any sharp yield point and transforms smoothly from yield to plastic region. After yielding, the dense composite exhibits work hardening phenomenon. Figure 6 (b) shows the deviation of plateau stresses, specific energy absorption along with relative densities at a diverse strain rate. It is evident that the relation between plateau stress and RD follows the power law irrespective of strain rate. The effect of higher strain rate is better than that of which is at lower strain rate and it also indicates the plateau stress does not follow any kind of precise trend with strain rate [19-20, 25].

The specific energy absorption with diverse foam has been calculated from their stress strain curves, which varies from 1.68MPa to 4.32MPa and the densities (0.77 to 1gmcc^{-1}) using the relationship in Eq. 1 [19]:

$$E_V = \frac{\left(\int_{\epsilon_0}^{\epsilon_d} \sigma d\epsilon\right)}{\rho} \quad (1)$$

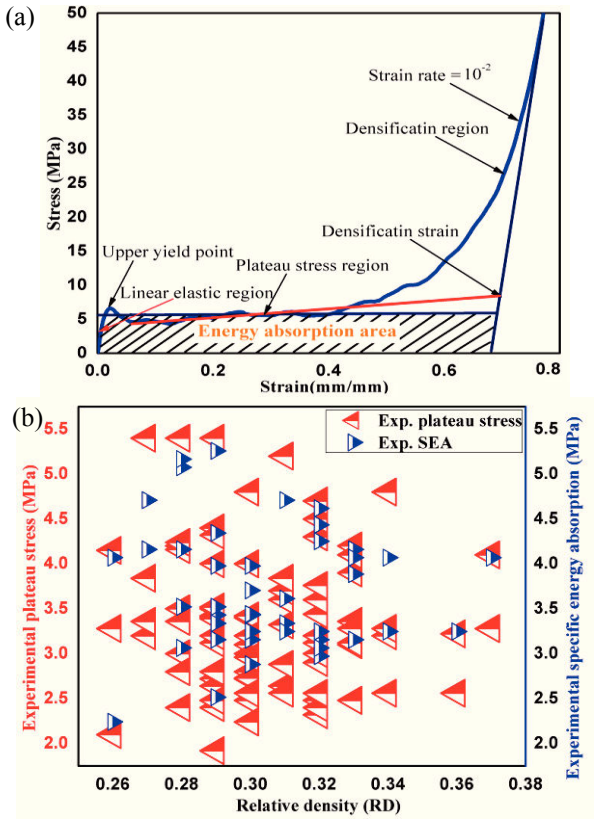

Fig. 6. (a) Stress-strain curve at a stain rate 10^{-2} s^{-1}, (b) experimental results between plateau stress, specific energy absorption and relative densities.

where E_v is specific energy absorption, σ_{pl} is the plateau stress; ρ is the density of material, ε_0 is the strain at zero deformation, ε_d is the strain at any instant of deformation (densification strain). The energy absorption (E_v) of the individual material was determined by superimposing fine grids on the stress strain curves and by counting the number of grids covered by the stress-strain curved up to desired strain level. The energy absorption by a single grid point is calculated from multiplication of its dimensions along stress axis with that along strain axis. The energy absorption of foams can be defined through the numerator of relation as stated in Eq. 1.The compression stress-strain curve for AAFs for various relative densities at fixed strain rate 10^{-2} s^{-1} is shown in Figure 7(a). This figure shows that the stable strain rate increases with increase in relative density (0.29 to 0.34) and Figure 7(b) shows the variation of compression stress-strain curve with stable relative density (0.29). It is evident from this curve that the plateau stress lies in small range with wider variation of strain rate (10^{-3} s^{-1} to 10 s^{-1}) [4, 12, 19-20].

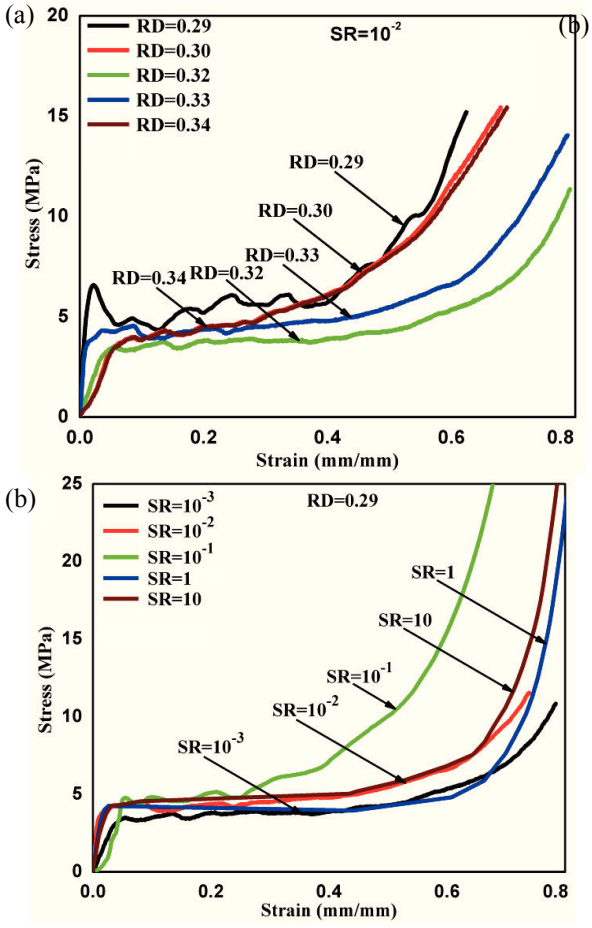

Fig. 7. (a) Compression stress-strain curve of AlSi17 alloy foam for various relative densities at fixed stain rate $10^{-2}s^{-1}$, (b) variation of compression stress-strain curve at diverse strain rates.

3.4. Artificial neural network (AAN) and simulation characterization

Artificial neural network is a study inspired from biological networks of human brain. Naturally the brain learns from experience in the same way we train the neural network to do certain actions. The basic building blocks of ANN are neurons. Each neurons works as shown in the Figure (8) for a neuron "i" the given inputs are x_1, x_2, x_3…. xn. Each input is weighted with wi_1, wi_2, wi_3, ….wi_n. These weighted inputs are summed along with a bias bi. These summation values are given as input to the transfer function f () of the neuron which gives output yi.

$$u_i = \sum_{i=1}^{n} w_{il} x_i + b_i \quad (2)$$

$$y_i = f(u_i) \quad (3)$$

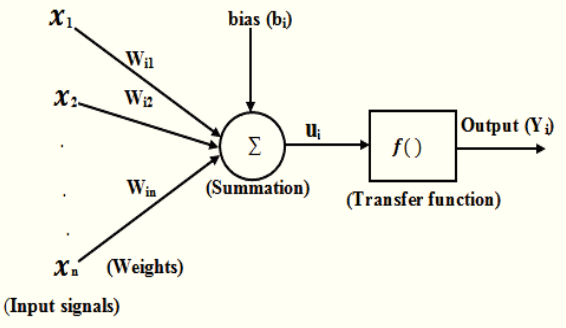

Fig. 8. A non-linear model of ANN.

A simple ANN model is characterized by an input layer, hidden layers and output layer. The input layer has several neurons which serve as inputs to the ANN. The output layer has one or more neurons depending upon the number of outputs required from the neural network. Hidden layers consist of several numbers number of neurons; these depend upon the accuracy of neural network. Each neuron is connected to all neurons in the previous layers by respective weights and computed using activation function like tansig, logsig, purelin etc. An approximate function is framed between the inputs and outputs by modifying the weights in the neural network by using back propagation algorithm. It is a mean square algorithm, which modifies weights (Eq. 5) in order to reduce the mean squared error (MSE) (Eq. 4) between the experimental values and outputs of ANN.

$$\mathrm{MSE} = \frac{1}{n}\sum_{i=1}^{n}(y_i - d_i)^2 \quad (4)$$

d_i= actual outputs

y_i= outputs of ANN

$$\Delta w_{il} = -\alpha \frac{\partial E}{\partial w_{il}} \quad (5)$$

Where $E = \frac{1}{2}(y - d)^2$

A feed-forward nature of neural network is used as shown in the Figure (9) in which the information flows in forward direction, from input neurons, through hidden neurons, to the output neurons. The strategy and training of AAN is done by changing the number of hidden layers, number of hidden neurons, transfer functions of the neurons, training function of the network and adaptive and learning functions of the network using neural network toolbar from MATLAB software.

The plateau stress values of the experimental analysis for 45 samples varying from 2.10 MPa to 5.4 MPa.

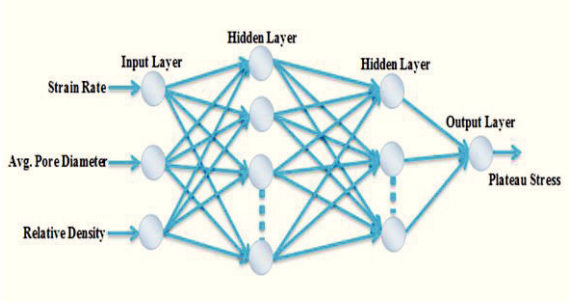

Fig. 9. Graphical presentation of the feed-forward ANN model.

The variable parameters for the 45 samples are strain rate, average pore diameter and relative density. The input processing parameters for ANN were listed in Table 2. In this ANN model feed-forward back propagation technique is used and is trained in MATLAB R2015a. It uses supervised learning for training the data with the use of inputs and outputs. A large number of neural networks are tested to train the neural network by changing the number of hidden layers, number of hidden neurons and the activation functions. The best topology is selected when the trained and tested data errors are satisfactory. The best topology for our ANN model is 3-10-1(3 neurons in input layer, 10 neurons in the hidden layer and 1 neuron in the output layer). The activation function used in the hidden layer neurons is 'logsig (Eq. 6)'; the activation function used in the output layer neuron is 'tansig (Eq. 7)'.

Logsig function:

$$f(x) = \frac{1}{1+e^{-x}} \quad (6)$$

Tansig function:-

$$tansig(x) = \left(\frac{2}{1+e^{-2x}}\right) - 1 \quad (7)$$

For training the neural network levenberg-Marquadt optimization method is used. The predicted plateau stress values through ANN are plotted against experimental values for studying correlation as shown in the Figure 10(a).The co-relation factor "R" obtained between predicted and target data is 0.9464, which shows very good resemblance between the predicted values and experimental values. The experimental value, predicted plateau stress values and average pore diameter is plotted against the samples as shown in the Figure 10(b).

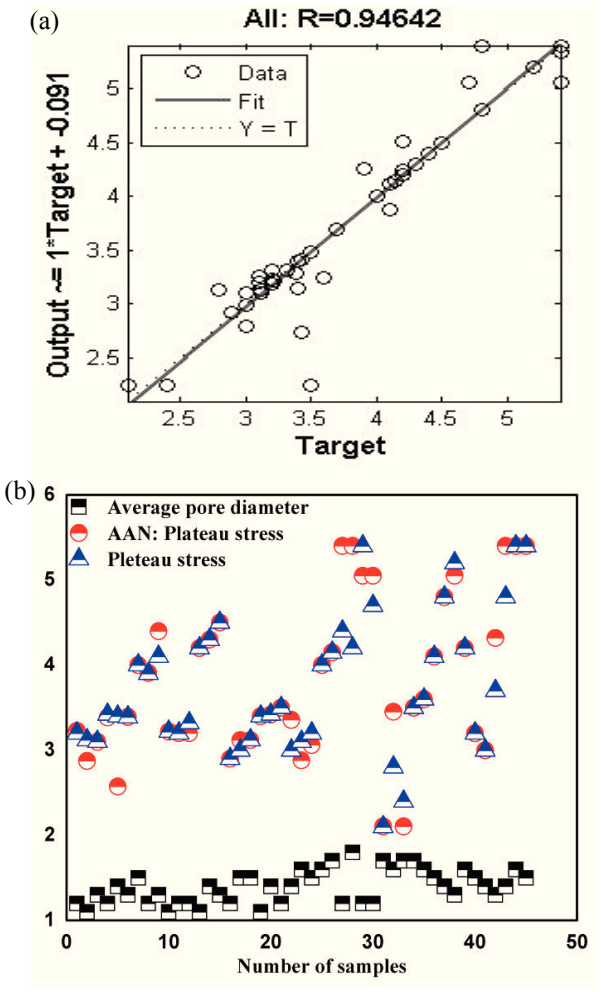

Fig.10. (a) Compared the simulated results with experimental of plateau stress with perfect line, (b) plateau stress variation both condition (experimental and AAN) with average pore diameter.

Table 2. Input processing parameters for ANN architecture.

Sl. no	Strain rate (s^{-1})	Average pore size (mm)	Relative density
1	0.001	1.2	0.29
2	0.001	1.2	0.29
3	0.001	1.3	0.30
4	0.001	1.4	0.31
5	0.001	1.4	0.31
6	0.001	1.3	0.30
7	0.001	1.5	0.32
8	0.001	1.4	0.32
9	0.001	1.3	0.30
10	0.01	1.6	0.33
11	0.01	1.3	0.30
12	0.01	1.4	0.31
13	0.01	1.4	0.31
14	0.01	1.3	0.30
15	0.01	1.7	0.34
16	0.01	1.7	0.34
17	0.01	1.6	0.33
18	0.01	1.4	0.32
19	0.1	1.2	0.29
20	0.1	1.8	0.34
21	0.1	1.2	0.29
22	0.1	1.6	0.33
23	0.1	1.6	0.33
24	0.1	1.5	0.32
25	0.1	1.5	0.32
26	0.1	1.2	0.29
27	0.1	1.4	0.31
28	1	1.6	0.33
29	1	1.3	0.30
30	1	1.5	0.32
31	1	1.9	0.34
32	1	1.8	0.34
33	1	1.9	0.34
34	1	1.3	0.30
35	1	1.4	0.31
36	1	1.2	0.29
37	10	1.3	0.30
38	10	1.2	0.29
39	10	1.5	0.32
40	10	1.3	0.30
41	10	1.2	0.29
42	10	1.5	0.32
43	10	1.4	0.31
44	10	1.3	0.30
45	10	1.6	0.33

4. Conclusions

The effect of strain rate on aluminum alloy (AlSi17) foam reinforced with 10%wt. SiC particle has been optimized under the compression loading conditions. The following conclusions can be drawn from the above study; Energy absorbing characteristic behavior of AlSi17alloy foam with different strain rate has been examined experimentally. These kinds of deformation procedure were observed during the crushing of foam. Most of aluminum alloy foam crushing ended to exhibit the regular mode collapse. The aluminum alloy foam has the maximum load

carrying ability and high energy absorption behaviour. AAN models are developed for the prediction of compressive properties (plateau stress) of AAFs by the help of experimental database. Maximum number of experimental data is established from the quasi-static compression test for analyzing the compression deformation behavior i.e. plateau stress separately and SEA capacity along with their mechanical properties. The input data selected for evolving the ANN model are the mechanical characteristics of AAFs i.e. the strain rate, average pore diameter and relative density. In the meantime using the ANN modeled higher co-relation factor "R" obtained between predicted and target data is 0.9464, which shows very good resemblance with the predicted values and experimental values.

Acknowledgements

One of the authors, Dipen Kumar Rajak, exhibits sincere thanks Light Weight Material Processing Laboratory AMPRI, Bhopal. The technical support offered for performing the experiments is highly appreciable. The authors also array a special thanks to Mr. Prasanth N., Technical Assistant, AMPRI, Bhopal for preparation of the samples.

References

[1] J. Banhart, Prog. Mater. Sci. 46 (2001) 559.
[2] J. Baumesister, J. Banhart, M. Weber, Mater. Des. 18 (1997) 217.
[3] J. Banhart, Int. J. Vehicle Des. 37 (2005) 114.
[4] D.K. Rajak, L.A. Kumaraswamidhas, S. Das, Mater. Sci. Tec. 32(13) (2016) 1345.
[5] R.E. Raj, B.S.S. Daniel, Comput. Mater. Sci. 43 (2008) 767.
[6] H. E. Kadi, Compos. Struct. 73 (2006) 1.
[7] D. K. Rajak, L.A. Kumaraswamidhas, S. Das, J. Mater. Eng. Perform. 25(8) (2016) 438.
[8] C. Z. Huang, L. Zhang, L. He, J. Sun, B. Fang, B. Zou, Z.Q. Li, L. Zhang, J. Mater. Process Technol. 129 (2002) 399.
[9] J. McBride, S. Malinov, W. Sha, Mater. Sci. Eng. A 384 (2004) 129.
[10] Z. Jiang, Z. Zhang, K. Friedrich, Compos. Sci. Technol. 67 (2007) 168.
[11] M. Li, X. Liu, A. Xiong, J. Mater. Process Technol. 121 (2002) 1.
[12] D.K. Rajak, L.A. Kumaraswamidhas, S. Das, Adv. Mater. Lett. 6(6) (2015) 548.
[13] Z. Zhang, K. Friedrich, Compos. Sci. Technol. 63 (2003) 2029.
[14] S. H. Hsiang, J.L. Kuo, Int. J. Adv. Manuf. Technol. 26 (2005) 970.
[15] E M. Bezerra, A.C. Ancelotti, L.C. Pardini, J.A.F.F. Rocco, K. Iha, C.H.C. Ribeiro, Mater. Sci. Eng. A 464 (2007) 177.
[16] S.M.K. Hosseini, A.Z. Hanzaki, M.J.Y. Parah, S. You, Mater. Sci. Eng. A 374 (2004) 122.
[17] H. Yu, Z. Guo, B. Li, G. Yao, H. Luo, Y. Liu, Mater. Sci. Eng. A 454-455 (2007) 542.
[18] C. Xiao-qing, W. Zhi-hua, M. Hong-wei, Z. Long-mao, Y. Gui-tong, Trans. Met. Sci. China 16 (2006) 351.
[19] D.K. Rajak, L.A. Kumaraswamidhas, S. Das, S.S. Kumararn, J. Alloys Compd. 656 (2016) 218.
[20] D.K. Rajak, L.A. Kumaraswamidhas, S. Das, Proc. Mater. Sci, 5 (2014) 164.
[21] A. Rabiei, T.A.O. Neill, Mater. Sci. Eng. A 404 (2005) 159.
[22] L.D. Kenny, Mater. Sci. Forum 217-222 (1996) 1883.
[23] V.S. Deshpande, N.A. Fleck, Int. J. Impact Eng. 24 (2000) 277.
[24] D.K. Rajak, L.A. Kumaraswamidhas, S. Das, Review. Adv. Mater. Sci. 48 (2017) 68.
[25] N. Orbulov, Mater. Sci. Eng. A 555 (2012) 52.
[26] A.E. Simone, L.J. Gibson, Acta Mater. 46(9) (1999) 3109.
[27] T. Miyoshi, M. Itoh, S. Akiyama, A. Kitahara, Adv. Eng. Mater. 2(4) (2000) 179.
[28] W. Deqing, S. Ziyuan, Mater. Sci. Eng. A 361 (2003) 45.